# Robust Beam-Alignment for TWDP Fading Millimeter Wave Channels

*(Invited Paper)*

Stefan Schwarz
*Christian Doppler Laboratory for Dependable Wireless Connectivity for the Society in Motion*
*TU Wien*
Vienna, Austria
sschwarz@nt.tuwien.ac.at

Erich Zöchmann
*Department of Radio Electronics*
*Brno University of Technology*
Brno, Czech Republic
ezoechma@nt.tuwien.ac.at

***Abstract*—In this paper, we consider hybrid transmit and receive beam-alignment in wireless millimeter wave transmissions. As several channel measurement campaigns have shown, the millimeter wave channel exhibits a limited number of scattering clusters, where each cluster can be well modeled by a small number of rays. To account for this behavior, we consider a clustered channel model with each cluster being modeled as two-wave with diffuse power (TWDP) fading. It is well known that TWDP fading can lead to worse outage performance than Rayleigh fading. We therefore propose several hybrid beam selection and power loading strategies to achieve robust transmission and we investigate their outage performance by means of Monte Carlo simulations.**

***Index Terms*—Beam Alignment, Outage Probability, Fading, TWDP, Millimeter Wave**

## I. Introduction

Wireless communications in millimeter wave (mmWave) frequency bands offers very high data rates [1]. Although antenna sizes at mmWaves are very small and allow for multiple antennas to be placed even in handheld devices, the high data rates are mainly based on the large available bandwidths at mmWaves. The degrees of freedom offered by the antenna arrays are commonly utilized to form narrow beams to enhance the receive power [2]. Thus, by utilizing narrow beams, the signal processing challenge of beam alignment comes into place [3]–[8].

Previously most of the work concentrated on non-fading channels and assumed a static gain for the interacting objects, where the beams were aligned to. The seminal work of [9] focused on the problem of fading clusters and addressed the problem by resorting to the estimation of the second order statistics. However, the authors of [9] assume a cluster to be Rayleigh fading, which contradicts a plurality of measurement campaigns; the work of [10]–[19] revealed that the channel has limited number of clusters where each cluster is modeled adequately with a few rays only. Rayleigh fading is hence not adequate to describe the small-scale fading once narrow beams are applied.

The financial support by the Austrian Federal Ministry for Digital and Economic Affairs and the National Foundation for Research, Technology and Development is gratefully acknowledged. The research described in this paper was co-financed by the Czech Science Foundation, Project No. 17-18675S Future transceiver techniques for the society in motion.

### *Our Contributions*

In this work we firstly propose a new, simple but yet accurate channel model to study the problem of robust beam alignment. Our channel model is based on a sum of two-wave with diffuse power (TWDP)-fading clusters. To achieve robustness against signal outages, a single data stream is transmitted over multiple beams and heuristic strategies are proposed to allocate power to each beam.

### *Notation*

We denote vectors and matrices by boldface lower- and upper-case letters $\mathbf{x}$ and $\mathbf{X}$. The conjugate-transpose of $\mathbf{X}$ is $\mathbf{X}^{\mathsf{H}}$ and the Frobenius norm is $\|\mathbf{X}\|$. We employ the notation $[\mathbf{X}]_{i,j}$ to access the $ij$-th element of matrix $\mathbf{X}$. The Kronecker-delta is $\delta_\ell$; i.e., $\delta_\ell = 1$ iff $\ell = 0$. The expected value of the random variable $r$ is $\mathbb{E}(r)$, its variance is $\mathrm{var}(r)$, and the probability of random event $\mathcal{A}$ is $\mathbb{P}(\mathcal{A})$.

## II. System Model

We consider single-user data transmission from a transmitter antenna array consisting of $N_t$ transmit antenna elements to a receiver antenna array consisting of $N_r$ receive antenna elements. We consider single-stream transmission and apply a hybrid beamforming strategy to enable a low-complexity transceiver implementation. Specifically, we assume that the transmitter and receiver apply analog filters $\mathbf{F}_t \in \mathbb{C}^{N_t \times N_\ell}$ and $\mathbf{F}_r \in \mathbb{C}^{N_r \times N_\ell}$ to align $N_\ell$ antenna beams along the strongest channel components. Additionally, the transmitter and receiver apply a digital beamformer $\mathbf{g}_t \in \mathbb{C}^{N_\ell \times 1}$ and receive filter $\mathbf{g}_r \in \mathbb{C}^{N_\ell \times 1}$, for data transmission and detection, respectively. The corresponding input-output relationship is:

$$y = \mathbf{g}_r^{\mathsf{H}} \mathbf{F}_r^{\mathsf{H}} \mathbf{H} \mathbf{F}_t \mathbf{g}_t x + \mathbf{g}_r^{\mathsf{H}} \mathbf{F}_r^{\mathsf{H}} \mathbf{n}, \tag{1}$$

where $\mathbf{n}$ denotes uncorrelated zero-mean complex-Gaussian receiver noise of variance $\sigma_n^2$, $x$ is the unit-power information

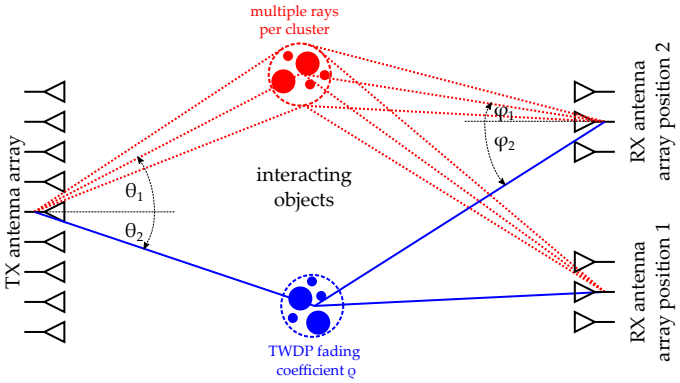


Fig. 1. Employed geometric channel model. Fading clusters are represented with a single ray whos path gain is drawn from a TWDP distribution. This avoids modeling the cluster with multiple rays and is well justified through measurements.

symbol and the digital filters are normalized as $\|\mathbf{g}_t\| = \|\mathbf{g}_r\| = 1$. We assume that the analog filters are implemented by phase-shifting elements, such that $\left|[\mathbf{F}_t]_{i,j}\right| = 1$, $\left|[\mathbf{F}_r]_{i,j}\right| = 1$, $\forall i, j$. We consider transmission over $N_\ell$ beams to improve the diversity and thus the robustness of the system.

### A. Channel Model

The channel model used in this study is a geometric channel model as commonly applied in mmWave and massive multiple-input multiple-output (MIMO) research [5], [9], [20]–[22]. The main assumption is that interacting objects are visible as clusters in the far field, see Fig 1. It has been found that clusters describe 3D MIMO channel models very well [23], [24]. The well known 3GPP 3D MIMO channel model [25] makes use of clusters described via a mean direction and a spread around this mean. By employing several rays the spatial extend of these clusters is modeled. By fixing the positions of the interacting objects, small-scale fading could be realized through varying the positions of the transmitter and/or the receiver. Such position variations alter the angles of the individual rays and thus the rays are summed with different phases. This effect is illustrated via the red cluster in Fig. 1. By moving from RX antenna array position 1 to RX antenna array position 2 several small-scale fading realizations are obtained.

However, we decided to abstract this superposition behavior through drawing the path gain from a specific distribution, as in [9]. As already mentioned, in [9], the random samples were chosen from a Rayleigh distribution, which seems rather unrealistic as the number of rays per cluster is typically small. Motivated through [19], the random path gain in this contribution is drawn from a TWDP distribution. The $l$-th complex cluster gain is hence modeled via:

$$\rho_l = \sqrt{\Omega_l}\left(V_1 \mathrm{e}^{\mathrm{j}\phi_1} + V_2 \mathrm{e}^{\mathrm{j}\phi_2} + X + \mathrm{j}Y\right) , \tag{2}$$

where $V_1 > 0$ and $V_2 \geq 0$ are the deterministic amplitudes of the non-fluctuating components and the phases $\phi_1, \phi_2$ are independent and uniformly distributed in $(0, 2\pi)$. The term $X + \mathrm{j}Y$ models numerous smaller contributions with the law of large numbers by drawing $X$ and $Y$ from $\mathcal{N}(0, \sigma_l^2)$. So, $\sigma_l^2$ denotes the variance of the real and the imaginary part of the diffuse scattering component. The $K$-factor is the power ratio of the non-fluctuating components and the diffuse component, similar to the Rician $K$-factor:

$$K = \frac{V_1^2 + V_2^2}{2\sigma_l^2} . \tag{3}$$

The variance $\sigma_l^2$ is chosen such that the second moment of the cluster gain is given by:

$$\mathbb{E}\left(|\rho_l|^2\right) = \Omega_l = 2\sigma_l^2(1 + K) . \tag{4}$$

Hence, $\sigma_l^2$ is given by:

$$\sigma_l^2 = \frac{\Omega_l}{2(1 + K)} . \tag{5}$$

The TWDP model has an additional parameter to model the relative strength of both non-fluctuating paths. This parameter is between 0 ($V_2 = 0$) and 1 ($V_1 = V_2$) and is calculated through:

$$\Delta = \frac{2V_1V_2}{V_1^2 + V_2^2} . \tag{6}$$

The amplitudes are thereby obtained as [26], [27]:

$$V_{1,2} = \sqrt{\frac{K\sigma_l^2}{2}}\left(\sqrt{1 + \Delta} \pm \sqrt{1 - \Delta}\right) . \tag{7}$$

W.l.o.g., we assume that clusters are sorted according to decreasing average power such that $\Omega_1 \geq \Omega_2 \geq \ldots \geq \Omega_L$. The variance of the powers of the TWDP paths is [28]:

$$\begin{aligned}\Theta_l &= \mathrm{var}\left(|\rho_l|^2\right) = \\ &= \frac{\Omega_l^2}{(1 + K)^2}\left(2 + 4K + K^2\left(1 + \frac{\Delta^2}{2}\right)\right) - \Omega_l^2 .\end{aligned} \tag{8}$$

We employ $\lambda/2$ spaced antenna arrays at both the transmitter and the receiver and assume isotropic radiation patterns in the plane of interest. The array response at the transmitter for a far-field wave impinging at an angle $\theta_l$ is given by:

$$\mathbf{a}(\theta_l) = [\mathrm{e}^{\mathrm{j}0\pi \sin\theta_l}, \mathrm{e}^{\mathrm{j}1\pi \sin\theta_l}, \ldots, \mathrm{e}^{\mathrm{j}N_t\pi \sin\theta_l}] , \tag{9}$$

the array response at the receiver at an angle of $\phi_l$ is equivalently given by:

$$\mathbf{b}(\phi_l) = [\mathrm{e}^{\mathrm{j}0\pi \sin\phi_l}, \mathrm{e}^{\mathrm{j}1\pi \sin\phi_l}, \ldots, \mathrm{e}^{\mathrm{j}N_r\pi \sin\phi_l}] . \tag{10}$$

The final channel model with $L$ clusters thus reads:

$$\mathbf{H} = \sum_{l=1}^{L} \rho_l \mathbf{b}(\phi_l)\mathbf{a}(\theta_l)^{\mathsf{H}} . \tag{11}$$

### B. Analog Filtering

We assume that the analog beamformers are updated relatively slowly based on macroscopic channel properties, i.e., based on the geometric angles of the dominant specular components. That is, the analog transmit and receive filters are matched to the antenna array response vectors of the $N_\ell$ specular components with largest average power $\Omega_l$. This is reasonable since, on the one hand, it is not feasible to estimate the full channel matrix $\mathbf{H}$ in each transmission time interval (TTI), and, on the other hand, state-of-the-art analog phase-shifters cannot be updated so quickly. For simplicity, we consider unquantized analog phase-shifters and thus obtain the analog filters as:

$$\mathbf{F}_t = \frac{1}{\sqrt{N_t}} \left[\mathbf{a}\big(\theta_1\big), \dots \mathbf{a}\big(\theta_{N_\ell}\big)\right], \tag{12}$$

$$\mathbf{F}_r = \frac{1}{\sqrt{N_r}} \left[\mathbf{b}\big(\phi_1\big), \dots \mathbf{b}\big(\phi_{N_\ell}\big)\right]. \tag{13}$$

### C. Digital Filtering

TWDP channels can exhibit very deep fading conditions, since the two specular components of the TWDP channel can add-up destructively. In our measurements reported in [19] at 60 GHz center frequency, we observed that the fading conditions can change dramatically when the position of the transmitter and/or receive antenna varies only by a few millimeters. It is thus necessary to exploit the diversity provided by the $N_\ell$ beams to improve the robustness of the data transmission. This can be accomplished by appropriate power loading using the digital transmit filter.

Since the fading is so sensitive w.r.t. the positioning and alignment of the transmit/receive antenna arrays it is, however, not reasonable to assume that the digital filters can be updated on a TTI-basis, at least not in frequency division duplex (FDD) systems, which have to rely on channel state information (CSI) feedback from the receivers. We thus assume that the digital transmit filters are calculated utilizing only channel statistics, as detailed in Section III.

For the digital receive filters an adaptation on a TTI-basis is reasonable, since the system anyway has to provide downlink pilot signals for channel estimation. We therefore employ maximum ratio combining (MRC) at the receiver:

$$\mathbf{g}_r = \frac{\mathbf{F}_r^{\mathsf{H}} \mathbf{H} \mathbf{F}_t \mathbf{g}_t}{\|\mathbf{F}_r^{\mathsf{H}} \mathbf{H} \mathbf{F}_t \mathbf{g}_t\|}. \tag{14}$$

We denote the product $\mathbf{h}_e = \mathbf{F}_r^{\mathsf{H}} \mathbf{H} \mathbf{F}_t \mathbf{g}_t$ as the effective channel.

## III. Transmit Power Loading Strategies

In this section, we investigate the design of the digital transmit filter in more detail. Since we apply MRC, the instantaneous output signal to noise ratio (SNR) $\beta$ of the receiver is:

$$\beta = \frac{\|\mathbf{h}_e\|^4}{\sigma_n^2\, \mathbf{h}_e^{\mathsf{H}} \mathbf{F}_r^{\mathsf{H}} \mathbf{F}_r \mathbf{h}_e}. \tag{15}$$

In general, the product $\mathbf{F}_r^{\mathsf{H}} \mathbf{F}_r$ is not equal to an identity matrix, complicating the analysis of the output SNR. To simplify the analysis, we assume that the directions of arrival are well separated such that $\mathbf{F}_r^{\mathsf{H}} \mathbf{F}_r \approx \mathbf{I}_{N_\ell}$ for $N_r$ large (large array approximation), leading to $\beta \approx \|\mathbf{h}_e\|^2 / \sigma_n^2$. Applying the same assumption at the transmitter-side, i.e. $\mathbf{F}_t^{\mathsf{H}} \mathbf{F}_t \approx \mathbf{I}_{N_\ell}$, implies:

$$\|\mathbf{h}_e\|^2 \approx \sum_{l=1}^{N_\ell} |\rho_l|^2 \, |[\mathbf{g}_t]_l|^2, \tag{16}$$

$$\beta \approx \frac{1}{\sigma_n^2} \sum_{l=1}^{N_\ell} |\rho_l|^2 \, |[\mathbf{g}_t]_l|^2. \tag{17}$$

### A. Average SNR Maximization

The approximate average SNR is

$$\mathbb{E}\,(\beta) \approx \frac{1}{\sigma_n^2} \sum_{l=1}^{N_\ell} \Omega_l \, p_l, \tag{18}$$

where the values $p_l = |[\mathbf{g}_t]_l|^2$ denote the transmit power-loading coefficients with total power constraint $\sum_{l=1}^{N_\ell} p_l = P_t$. The approximate average SNR is maximized by allocating all transmit power to the strongest beam, i.e., setting $p_l = P_t \, \delta_{l-1}$.

### B. Outage-Based Transmit Beam Selection

The SNR (17) is determined by the weighted sum of the squares of the TWDP fading random variables $|\rho_l|$ and, thus, the outage probability $\mathbb{P}\,(\beta < \beta_t)$ is a function of the power allocation $p_l$. The probability density function (pdf) of the sum of independent random variables is obtained from the convolution of the individual pdfs. To the best of our knowledge, this distribution is in closed-form not available for the sum of squared TWDP random variables.

We thus resort to transmit beam selection:

$$p_l = P_t \, \delta_{l - i_{\min}}, \tag{19}$$

$$i_{\min} = \underset{\ell \in \{1,\dots,N_\ell\}}{\arg\min} \;\; \mathbb{P}\left(\Omega_\ell < \beta_t \, \sigma_n^2\right). \tag{20}$$

The outage probability of each beam can be calculated from the well-known integral cumulative distribution function (cdf) expression of TWDP fading [29].

### C. Minimum Variance Power Allocation

The variance of the squared-norm of the effective channel vector is:

$$\mathrm{var}\left(\|\mathbf{h}_e\|^2\right) \approx \sum_{l=1}^{N_\ell} \Theta_l \, p_l^2, \tag{21}$$

and thus depends on the power allocation. Based on this observation, we propose the following variance minimization:

$$\begin{aligned} \min_{p_l \in \mathbb{R}} \;\; & \sum_{l=1}^{N_\ell} \Theta_l \, p_l^2 \\ \text{s.t.} \;\; & p_l \geq 0, \forall l \in \{1, \dots, N_\ell\}, \\ & \sum_{l=1}^{N_\ell} p_l = P_t, \\ & \sum_{l=1}^{N_\ell} \Omega_l \, p_l \geq \gamma_t s_p, \end{aligned} \tag{22}$$

where $\gamma_t = \beta_t \sigma_n^2$ denotes the minimum receive power threshold, equivalent to the minimum receive SNR threshold $\beta_t$. The goal of this optimization problem is to minimize the fading of the effective channel, while ensuring that the average power does not fall below the constraint $\gamma_t s_p$, where the power scaling $s_p$ is a tuning parameter. This quadratic program can be solved by any state-of-the-art convex optimization tool. The problem is infeasible in case $\Omega_1 < \gamma_t s_p$; in this case we set $p_l = P_t \delta_{l-1}$ to maximize the average received power.

## IV. Results

In this section, we investigate the performance of the proposed transmit power loading strategies. We consider $N_t = N_r = 64$ transmit and receive antennas, $L = 3$ paths, $N_\ell = 3$ beams and a receive SNR threshold of $\beta_t = 0\,\text{dB}$. We assume that the transmit and receive angles $\theta_l$ and $\phi_l$ are uniformly distributed in $[-\pi, \pi]$.

We consider the following $K$ and $\Delta$ parameters for the TWDP random variables: $[K_1, K_2, K_3] = [1, 10, 50]$, $[\Delta_1, \Delta_2, \Delta_3] = [1, 0.5, 0.1]$. We furthermore assume $\sum_{l=1}^{L} \Omega_l = 1$ and set $\Omega_2/\Omega_1 = 1/2$ and $\Omega_3/\Omega_1 = 1/5$. These seemingly random choices have been selected to achieve strongly different fading behavior over the three individual beams, as we will see below in the simulation results.

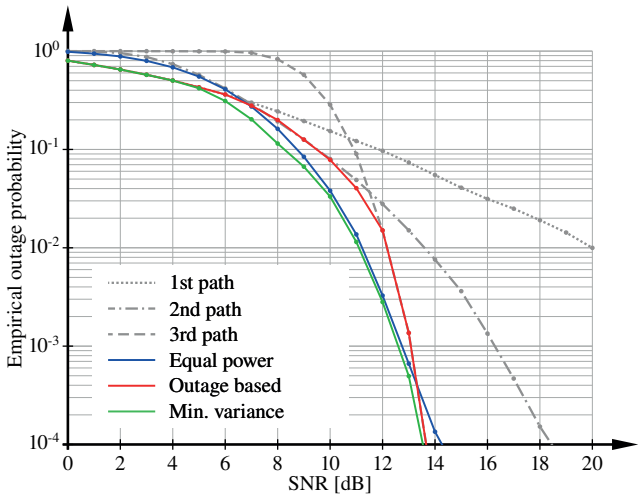


Fig. 2. Comparison of the empirical outage probability of several power allocation/beam selection strategies as a function of the SNR.

In Fig. 2, we investigate the outage behavior of several transmit power allocation/beam selection strategies as a function of the transmit SNR $P_t/\sigma_n^2$. We consider transmission over the three individual beams by setting the corresponding transmit power $p_1$, $p_2$ or $p_3$ equal to $P_t$ (notice, $p_1 = P_t$ corresponds to the maximum average SNR power allocation), equal power allocation $p_l = P_t/3$, $\forall l$, as well as, outage-based transmit beam selection and minimum variance power allocation with power scaling factor $s_p = 2$. When transmitting over the three individual beams, we observe the distinct fading behavior of the corresponding paths: the first path has large average power

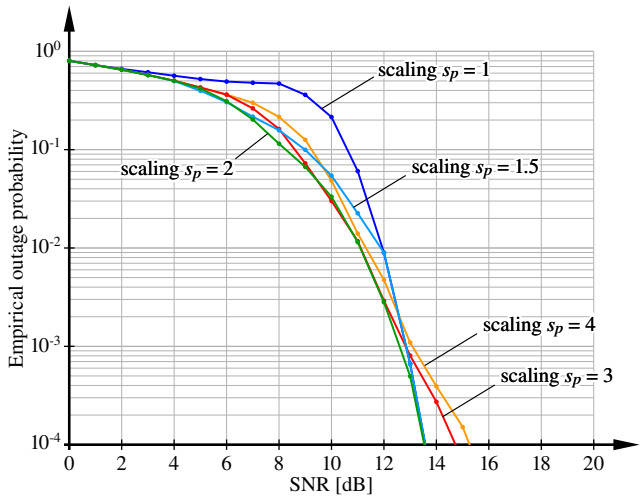


Fig. 3. Empirical outage probability of the variance minimization strategy with different power scaling factors $s_p$.

but strong fading, the third path has weak average power but hardly any fading and the second path lies in-between. The outage-based beam selection follows the minimum of these three curves. The equal power allocation strategy performs better than the outage-based beam selection in the intermediate SNR regime, where the individual outage probabilities of the three beams are not too dissimilar. The best performance is achieved by our proposed minimum variance power allocation with power scaling $s_p = 2$.

However, the performance of the minimum variance power allocation depends on the choice of the tuning parameter $s_p$. This is investigated in Fig. 3, where we show the performance of the minimum variance power allocation for different power scaling parameters $s_p \in \{1, 1.5, 2, 3, 4\}$. The variation in the outage behavior for $s_p \in [1.5, 4]$ is relatively small; yet, we cannot claim that this is true for any general scenario. Hence, providing a general guideline for the selection of $s_p$ is an important future work.

## V. Conclusion

Wireless transmissions in the mmWave band rely on antenna arrays or directional antennas to achieve sufficient signal power at the receivers. The directional antenna gain pattern thereby acts as a spatial filter that effectively reduces the number of relevant rays within a scattering cluster to a small value. To represent this behavior, we proposed to utilize a clustered channel model, where each scattering cluster follows a TWDP fading statistic. As the TWDP fading model can exhibit fading conditions that are even worse than Rayleigh fading, it is important to exploit the macroscopic diversity provided by beamforming over multiple scattering clusters to achieve an acceptable outage performance. To this end, we proposed several low complexity hybrid beam-alignment and power allocation strategies to improve the robustness of mmWave transmissions. Our future work includes a further in-depth investigation of the outage probability of the involved

weighted sum of TWDP fading random variables, to derive the analytic outage probability as a basis for an outage optimal power allocation strategy. Furthermore, we plan to extend the investigation to single-user as well as multi-user spatial multiplexing.

## REFERENCES


[1] Z. Pi and F. Khan, "An introduction to millimeter-wave mobile broadband systems," *IEEE Communications Magazine*, vol. 49, no. 6, pp. 101–107, 2011.

[2] R. W. Heath, N. Gonzalez-Prelcic, S. Rangan, W. Roh, and A. M. Sayeed, "An overview of signal processing techniques for millimeter wave MIMO systems," *IEEE Journal of Selected Topics in Signal Processing*, vol. 10, no. 3, pp. 436–453, 2016.

[3] S. Hur, T. Kim, D. J. Love, J. V. Krogmeier, T. A. Thomas, and A. Ghosh, "Millimeter wave beamforming for wireless backhaul and access in small cell networks," *IEEE Transactions on Communications*, vol. 61, no. 10, pp. 4391–4403, 2013.

[4] H. Shokri-Ghadikolaei, L. Gkatzikis, and C. Fischione, "Beam-searching and transmission scheduling in millimeter wave communications," in *Proc. of IEEE International Conference on Communications (ICC)*, 2015, pp. 1292–1297.

[5] E. Zöchmann, S. Schwarz, and M. Rupp, "Comparing antenna selection and hybrid precoding for millimeter wave wireless communications," in *Proc. of IEEE Sensor Array and Multichannel Signal Processing Workshop (SAM)*. IEEE, 2016, pp. 1–5.

[6] S. Noh, M. D. Zoltowski, and D. J. Love, "Multi-resolution codebook and adaptive beamforming sequence design for millimeter wave beam alignment," *IEEE Transactions on Wireless Communications*, vol. 16, no. 9, pp. 5689–5701, 2017.

[7] C. Perfecto, J. Del Ser, and M. Bennis, "Millimeter-wave V2V communications: Distributed association and beam alignment," *IEEE Journal on Selected Areas in Communications*, vol. 35, no. 9, pp. 2148–2162, 2017.

[8] C. Liu, M. Li, S. V. Hanly, I. B. Collings, and P. Whiting, "Millimeter wave beam alignment: Large deviations analysis and design insights," *IEEE Journal on Selected Areas in Communications*, vol. 35, no. 7, pp. 1619–1631, 2017.

[9] X. Song, S. Haghighatshoar, and G. Caire, "A scalable and statistically robust beam alignment technique for mm-wave systems," *IEEE Transactions on Wireless Communications*, 2018.

[10] E. Zöchmann, M. Lerch, S. Caban, R. Langwieser, C. Mecklenbräuker, and M. Rupp, "Directional evaluation of receive power, Rician K-factor and RMS delay spread obtained from power measurements of 60 GHz indoor channels," in *Proc. of IEEE Topical Conference on Antennas and Propagation in Wireless Communications (APWC)*, 2016, pp. 1–4.

[11] E. Zöchmann, M. Lerch, S. Pratschner, R. Nissel, S. Caban, and M. Rupp, "Associating spatial information to directional millimeter wave channel measurements," in *Proc. of IEEE Vehicular Technology Conference (VTC-Fall)*, 2017, pp. 1–5.

[12] E. Zöchmann, K. Guan, and M. Rupp, "Two-ray models in mmWave communications," in *Proc. of IEEE 18th International Workshop on Signal Processing Advances in Wireless Communications (SPAWC)*, 2017, pp. 1–5.

[13] N. Iqbal, D. Dupleich, C. Schneider, J. Luo, R. Müller, S. Häfner, G. Del Galdo, and R. S. Thomä, "Modeling of intra-cluster multipaths for 60 GHz fading channels," in *Proc. of the 12th European Conference on Antennas and Propagation (EuCAP)*, 2018.

[14] E. Zöchmann, C. F. Mecklenbräuker, M. Lerch, S. Pratschner, M. Hofer, D. Löschenbrand, J. Blumenstein, S. Sangodoyin, G. Artner, S. Caban, T. Zemen, A. Prokes, M. Rupp, and A. F. Molisch, "Measured delay and Doppler profiles of overtaking vehicles at 60 GHz," in *Proc. of the 12th European Conference on Antennas and Propagation (EuCAP)*, 2018, pp. 1–5.

[15] N. Iqbal, J. Luo, D. Dupleich, S. Häfner, R. Müller, C. Schneider, and R. S. Thomä, "Second-order statistical characterization of the 60 GHz cluster fading channels," in *Proc. of IEEE 29th Annual International Symposium on Personal, Indoor and Mobile Radio Communications (PIMRC)*. IEEE, 2018, pp. 241–245.

[16] E. Zöchmann, C. Mecklenbräuker, M. Lerch, S. Pratschner, M. Hofer, D. Löschenbrand, J. Blumenstein, S. Sangodoyin, G. Artner, S. Caban, T. Zemen, A. Prokes, M. Rupp, and A. F. Molisch, "Measured delay and Doppler profiles of overtaking vehicles at 60 GHz," in *Proc. of the 12th European Conference on Antennas and Propagation (EuCAP)*. IEEE, 2018, pp. 1–5.

[17] N. Iqbal, J. Luo, R. Müller, G. Steinböck, C. Schneider, D. Dupleich, S. Häfner, and R. S. Thomä, "Multipath cluster fading statistics and modeling in millimeter wave radio channels," *IEEE Transactions on Antennas and Propagation*, 2019.

[18] E. Zöchmann, M. Hofer, M. Lerch, S. Pratschner, L. Bernadó, J. Blumenstein, S. Caban, S. Sangodoyin, H. Groll, T. Zemen, A. Prokeš, M. Rupp, A. F. Molisch, and C. F. Mecklenbräuker, "Position-specific statistics of 60 GHz vehicular channels during overtaking," *IEEE Access*, pp. 1–1, 2019.

[19] E. Zöchmann, S. Caban, C. F. Mecklenbräuker, S. Pratschner, M. Lerch, S. Schwarz, and M. Rupp, "Better than Rician: modelling millimetre wave channels as two-wave with diffuse power," *EURASIP Journal on Wireless Communications and Networking*, vol. 2019, no. 1, pp. 1–21, 2019.

[20] Q. H. Spencer, B. D. Jeffs, M. A. Jensen, and A. L. Swindlehurst, "Modeling the statistical time and angle of arrival characteristics of an indoor multipath channel," *IEEE Journal on Selected Areas in Communications*, vol. 18, no. 3, pp. 347–360, 2000.

[21] S. Schwarz, "Outage-based multi-user admission control for random-phase finite-scatterer MISO channels," in *Proc. of IEEE Vehicular Technology Conference (VTC-Fall)*, Toronto, Canada, Sept. 2017, pp. 1–5.

[22] ——, "Outage investigation of beamforming over random-phase finite-scatterer MISO channels," *IEEE Signal Processing Letters*, 2017.

[23] S. Sangodoyin, V. Kristem, C. Bas, M. Käske, J. Lee, C. Schneider, G. Sommerkorn, J. Zhang, R. Thomä, and A. Molisch, "Cluster characterization of 3D MIMO propagation channel in an urban macrocellular environment," *IEEE Transactions on Wireless Communications*, 2018.

[24] C. Ling, X. Yin, R. Müller, S. Häfner, D. Dupleich, C. Schneider, J. Luo, H. Yan, and R. Thomä, "Double-directional dual-polarimetric cluster-based characterization of 70–77 GHz indoor channels," *IEEE Transactions on Antennas and Propagation*, vol. 66, no. 2, pp. 857–870, 2018.

[25] F. Ademaj, M. Taranetz, and M. Rupp, "3GPP 3D MIMO channel model: a holistic implementation guideline for open source simulation tools," *EURASIP Journal on Wireless Communications and Networking*, vol. 2016, no. 1, p. 55, 2016.

[26] T. Mavridis, L. Petrillo, J. Sarrazin, A. Benlarbi-Delai, and P. De Doncker, "Near-body shadowing analysis at 60 GHz," *IEEE Transactions on Antennas and Propagation*, vol. 63, no. 10, pp. 4505–4511, 2015.

[27] D. Kim, H. Lee, and J. Kang, "Comments on "Near-body shadowing analysis at 60 GHz"," *IEEE Transactions on Antennas and Propagation*, vol. 65, no. 6, pp. 3314–3314, 2017.

[28] M. Rao, F. J. Lopez-Martinez, M.-S. Alouini, and A. Goldsmith, "MGF approach to the analysis of generalized two-ray fading models," *IEEE Transactions on Wireless Communications*, vol. 14, no. 5, pp. 2548–2561, 2015.

[29] G. D. Durgin, T. S. Rappaport, and D. A. De Wolf, "New analytical models and probability density functions for fading in wireless communications," *IEEE Transactions on Communications*, vol. 50, no. 6, pp. 1005–1015, 2002.